Electronic Supplementary Material (ESI) for Dalton Transactions.

Supplementary Information For:

A Functionalized UiO-66 MOF for Turn-On Fluorescent Sensing of Superoxide in Water and Efficient Catalysis of Knoevenagel Condensation

Aniruddha Das,[a] Nagaraj Anbu,[b] Mostakim SK,[a] Amarajothi Dhakshinamoorthy[b] and Shyam Biswas*[a]*

[a] Department of Chemistry, Indian Institute of Technology Guwahati, Guwahati, 781039 Assam, India. E-mail: sbiswas@iitg.ernet.in

[b] School of Chemistry, Madurai Kamaraj University, Madurai 625021, Tamil Nadu, India. E-mail: admguru@gmail.com

* To whom correspondence should be addressed. E-mail: sbiswas@iitg.ernet.in; admguru@gmail.com.

Materials and Characterization Methods:

The 2-((pyridin-4-ylmethyl)amino)terephthalic acid (H_2BDC-NH-CH_2-Py) linker was synthesized and characterized (Figure S1-S3, Supporting Information) by following the procedure described below. All the chemicals were purchased from commercial sources and used without further purification. Fourier transform infrared (FT-IR) spectroscopy data were recorded in the region 400-4000 cm^{-1} at room temperature with the Perkin Elmer Spectrum Two FT-IR spectrometer. The following indications were used to indicate the corresponding absorption bands: very strong (vs), strong (s), medium (m), weak (w), shoulder (sh) and broad (br). Thermogravimetric (TG) experiments were carried out with a heating rate of 10 °C min^{-1} under argon atmosphere using using a SDT Q600 thermogravimetric analyzer. XRPD data were collected in transmission mode using a Bruker D2 Phaser X-ray diffractometer (30 kV, 10 mA) using Cu-Kα (λ = 1.5406 Å) radiation. Specific surface area for N_2 sorption was calculated on a Quantachrome Autosorb iQMP gas sorption analyzer at -196 °C. The compound was activated at 100 °C for 24 h under dynamic vacuum. Fluorescence emission studies were performed at room temperature using a HORIBA JOBIN YVON Fluoromax-4 spectrofluorometer. UV-vis spectra in the region 250–800 nm were recorded using a Perkin Elmer Lambda 25 UV-vis spectrometer. All solutions for the UV-vis measurements were prepared by using Milli-Q water. For catalytic investigations, the conversion and selectivity were determined with the help of Agilent 7820A gas chromatograph using nitrogen as carrier gas. The products were confirmed by analyzing the reaction mixture with Agilent 5890 GC-MS.

Synthesis of H_2BDC-NH-CH_2-Py Linker:

The below-mentioned synthetic procedure was followed during the synthesis of the H_2BDC-NH-CH_2-Py linker.

(E)-2-((pyridin-4-ylmethylene)amino)terephthalic acid[1] (1.60 g, 6 mmol) was dissolved in 50 mL of DMF and stirred at room temperature until complete dissolution was achieved. After that $NaBH_3CN$ (0.60 g, 9.00 mmol) was added to the mixture at 0 °C and kept under stirring conditions at 0 °C for 6 h. After 6 h, the reaction mixture was poured onto crushed ice in a 250 mL beaker and kept for 5 h to achieve complete precipitation of the yellow colored product. Finally, the precipitate was collected by vacuum filtration, followed by washing with sufficient amount of water and drying in a conventional oven at 80 °C for 12 h. Yield: 0.8 g (2.93 mmol, 50%). ^{1}H NMR (400 MHz, DMSO-d_6): δ = 8.62 (d, 2H), 7.94 (d, 1H), 7.78 (d, 1H), 7.15 (dd, 1H), 6.98 (d, 1H), 4.82 (s, 2H) ppm. ^{13}C NMR (100 MHz, DMSO-d_6): δ = 169.79, 167.31, 157.45, 150.00, 147.62, 136.26, 132.73, 125.20, 116.18, 114.83, 112.45 ppm. ESI-MS (m/z): 273.08 for $(M+H)^+$ ion (M = mass of H_2BDC-$C_6H_7N_2$ linker). In Figures S1-S3 (Supporting Information), the NMR and mass spectra for the H_2BDC-NH-CH_2-Py linker are shown.

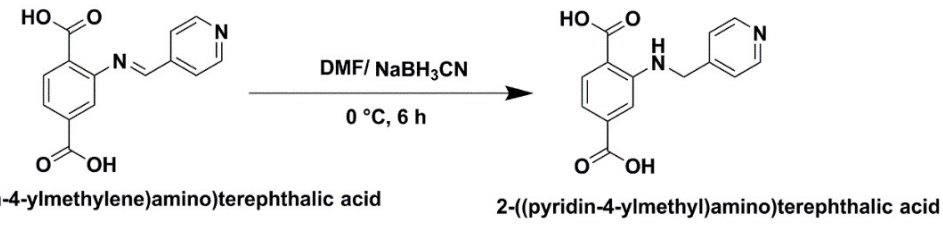

Scheme S1. Reaction scheme for the preparation of H_2BDC-NH-CH_2-Py linker.

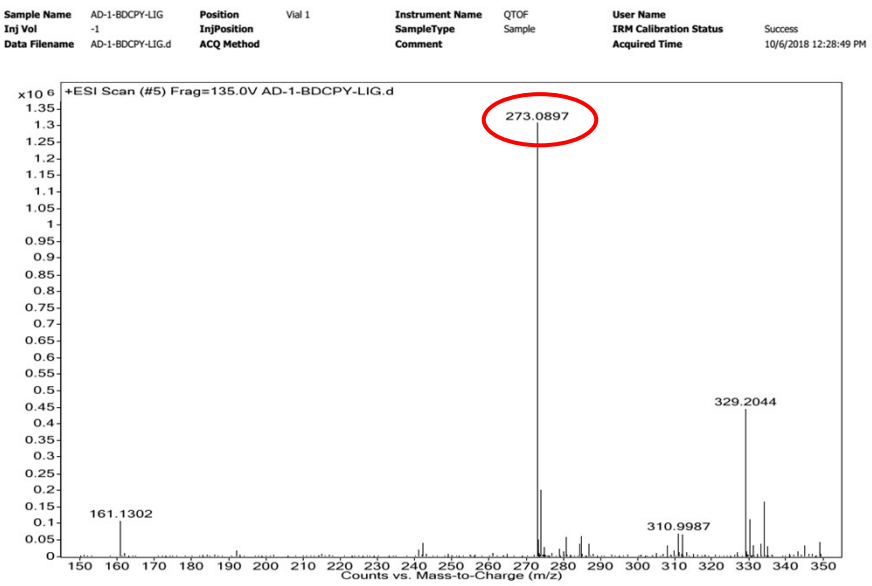

Figure S1. ESI-MS spectrum of the $H_2BDC\text{-}C_6H_7N_2$ linker in methanol. The spectrum shows m/z (positive ion mode) peak at 273.08, which corresponds to $(M+H)^+$ ion (M = mass of $H_2BDC\text{-}C_6H_7N_2$ linker).

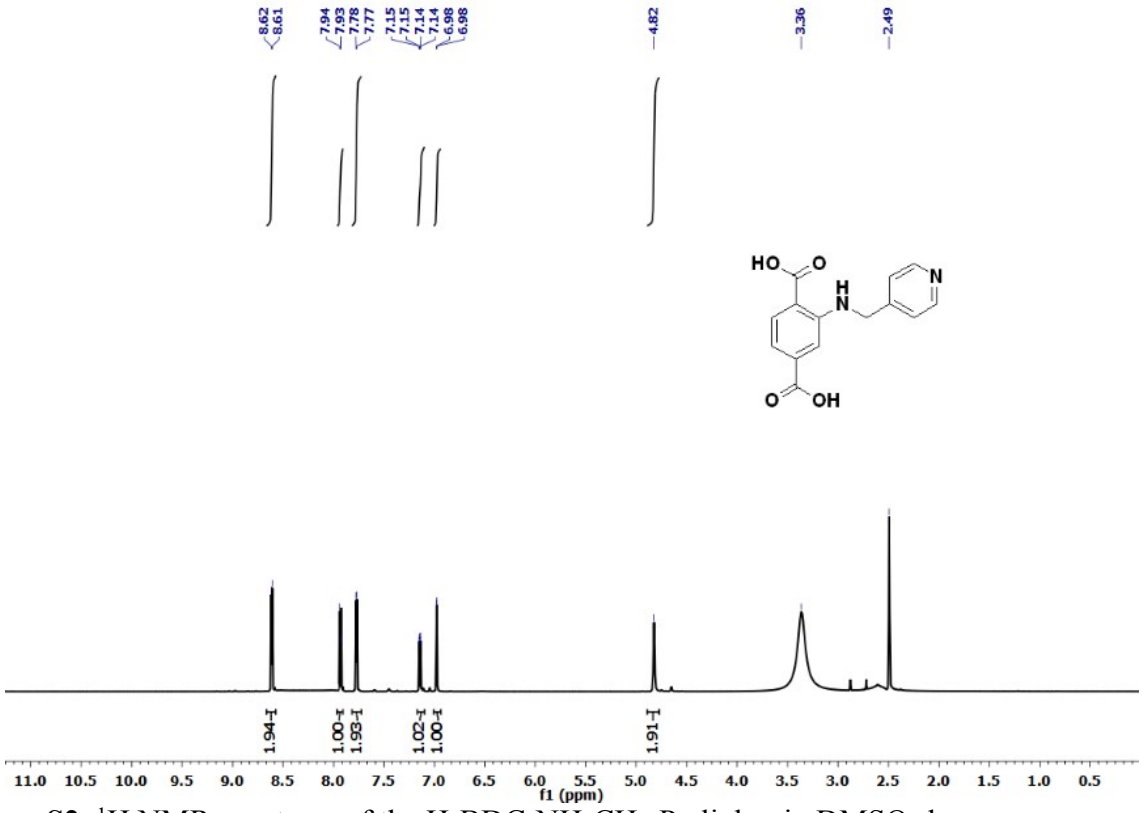

Figure S2. ^1H NMR spectrum of the $H_2BDC\text{-}NH\text{-}CH_2\text{-}Py$ linker in DMSO-d_6.

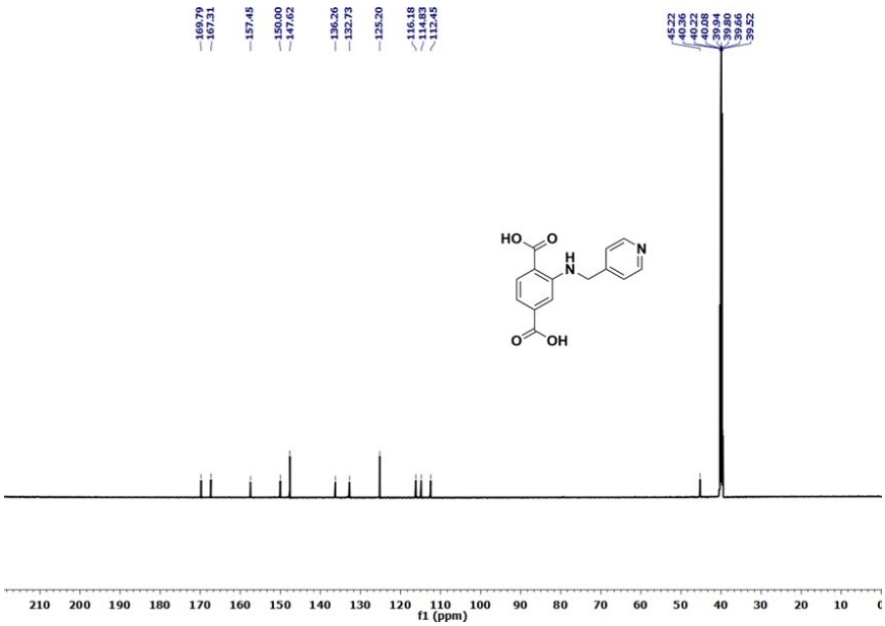

Figure S3. ^{13}C NMR spectrum of the $H_2BDC\text{-}NH\text{-}CH_2\text{-}Py$ linker in DMSO-d_6.

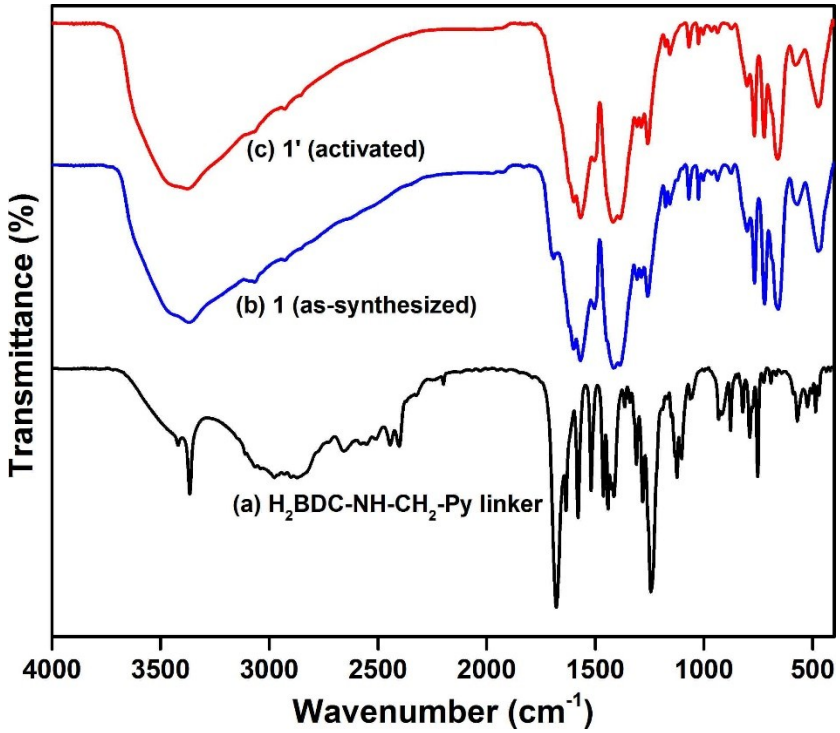

Figure S4. FT-IR spectra of (a) $H_2BDC\text{-}NH\text{-}CH_2\text{-}Py$ linker, (b) **1** (as-synthesized) and (c) **1′** (activated).

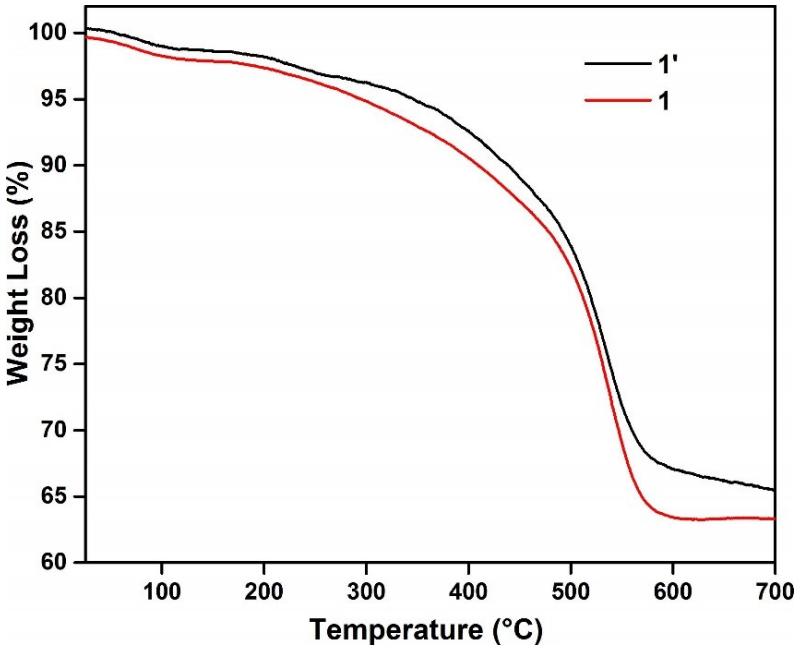

Figure S5. TG curves of as-synthesized **1** (red) and thermally activated **1′** (black) recorded under argon atmosphere in the temperature range of 25-700 °C with a heating rate of 10 °C min^{-1}.

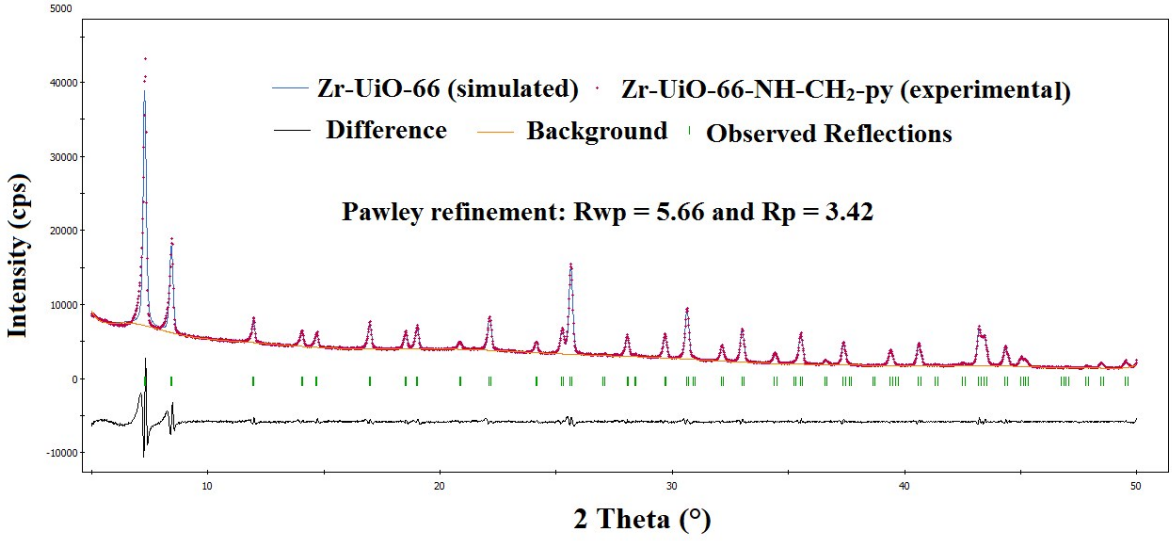

Figure S6. Pawley fit for the XRPD pattern of as-synthesized **1**. Blue lines and red dots denote calculated and observed patterns, respectively. The peak positions and difference plot are displayed at the bottom (R_{wp} = 5.66, R_p = 3.42).

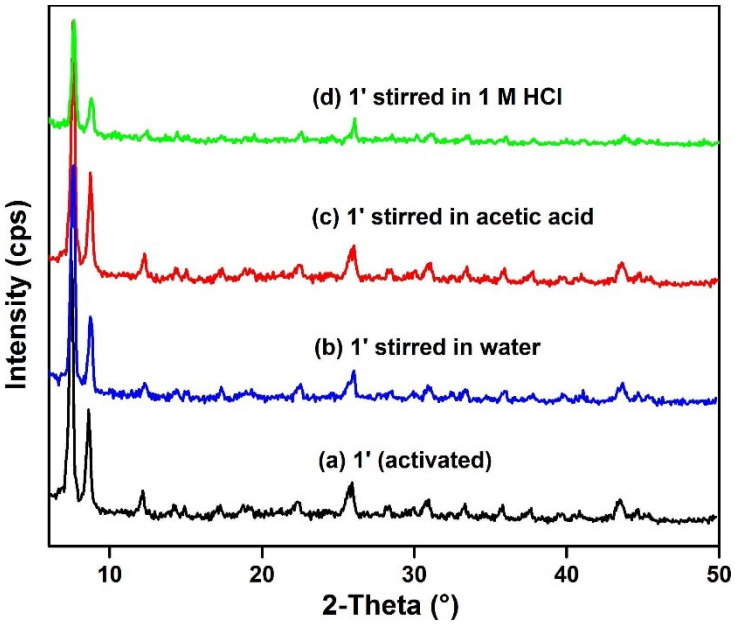

Figure S7. XRRD patterns of **1′** under different conditions: (a) activated, (b) after stirring in water, (c) after stirring in acetic acid and (d) after stirring in 1 M HCl.

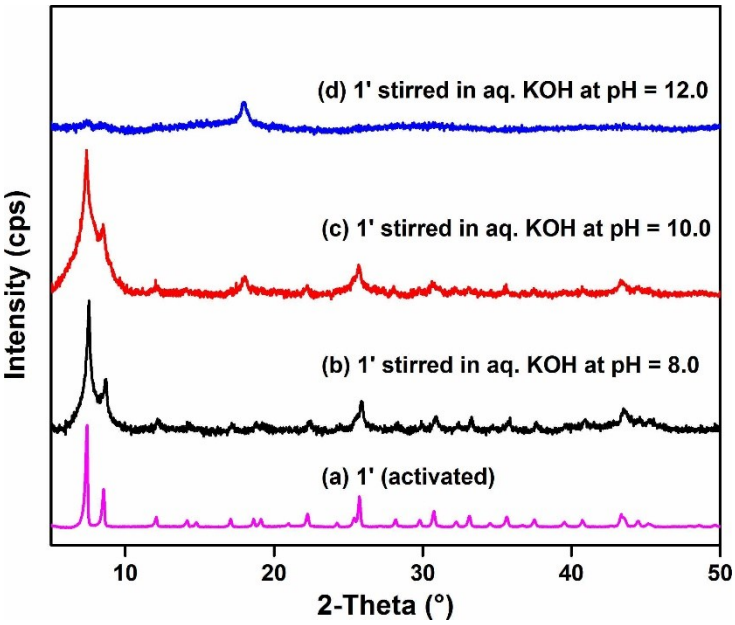

Figure S8. XRRD patterns of **1′** under different conditions: (a) activated, (b) after stirring in aqueous solution of KOH at pH = 8.0, (c) after stirring in aqueous solution of KOH at pH = 10.0 and (d) after stirring in aqueous solution of KOH at pH = 12.0.

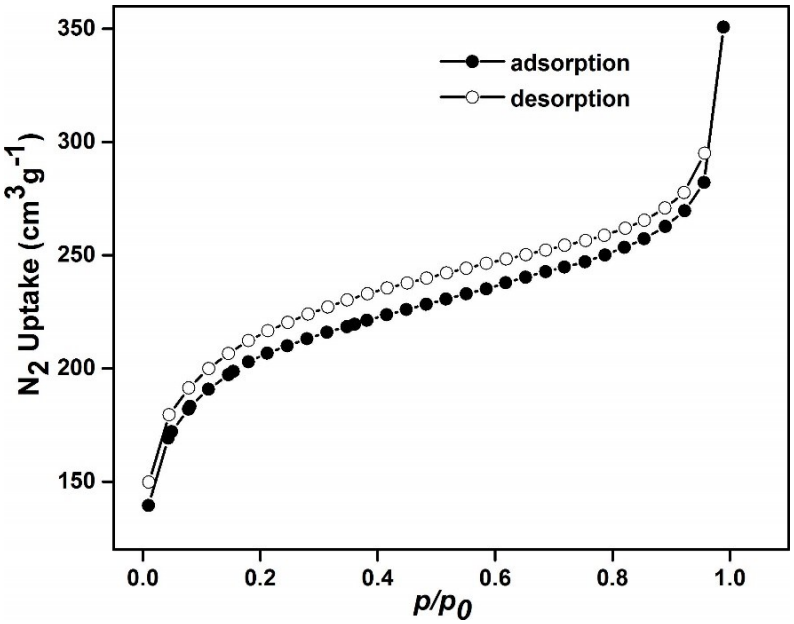

Figure S9. N_2 adsorption (solid circles) and desorption (empty circles) isotherms of **1′** measured at –196 °C.

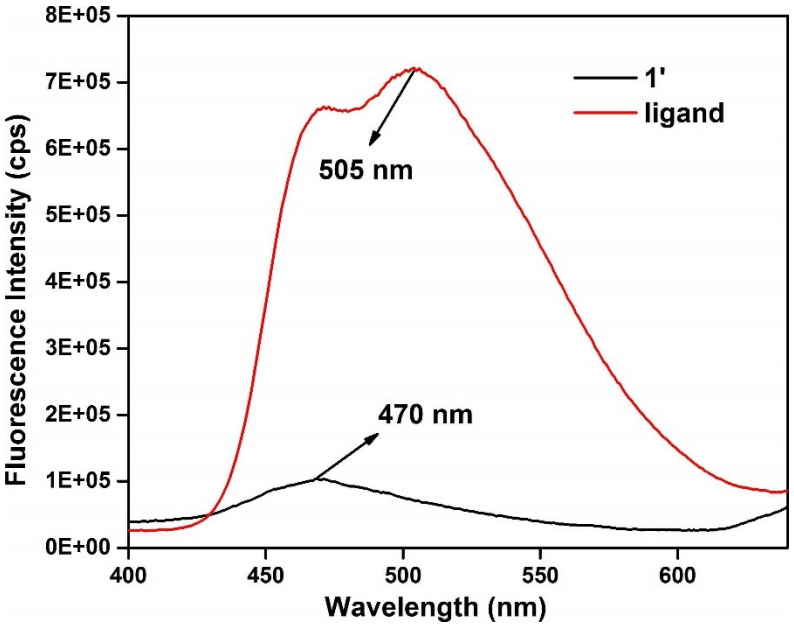

Figure S10. Solid state fluorescence spectra of **1′** and free H_2BDC-NH-CH_2-Py linker (λ_{ex} = 330 nm).

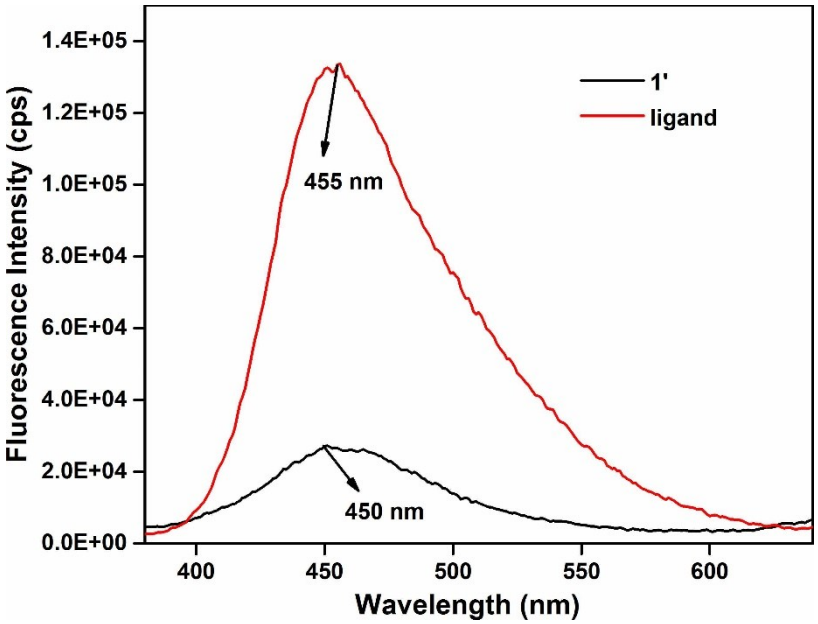

Figure S11. Comparison of fluorescence emission spectra of **1′** and free $H_2BDC\text{-}NH\text{-}CH_2\text{-}Py$ linker in aqueous medium (λ_{ex} = 330 nm).

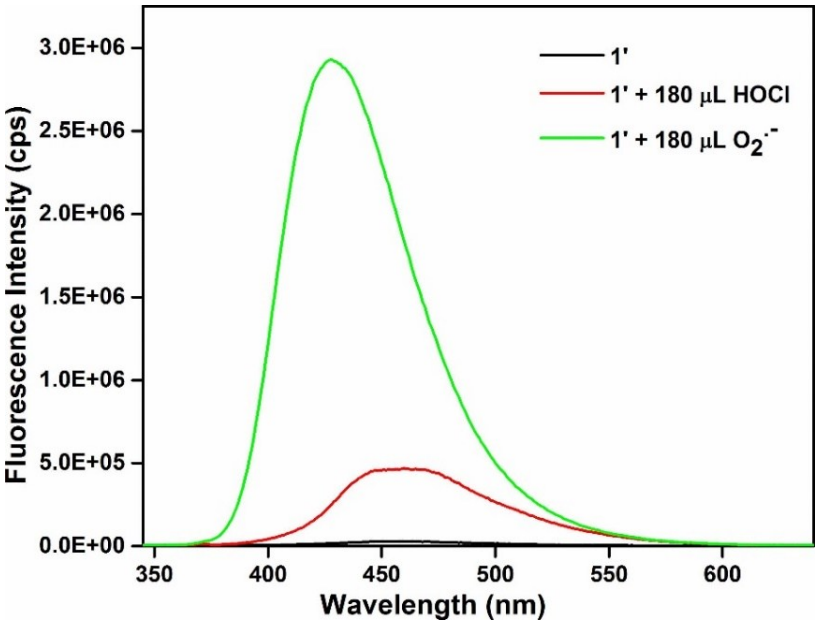

Figure S12. Change in the fluorescence intensity of **1′** upon addition of 10 mM HOCl solution (180 µL) in presence of 10 mM $O_2^{\bullet-}$ (180 µL) solution.

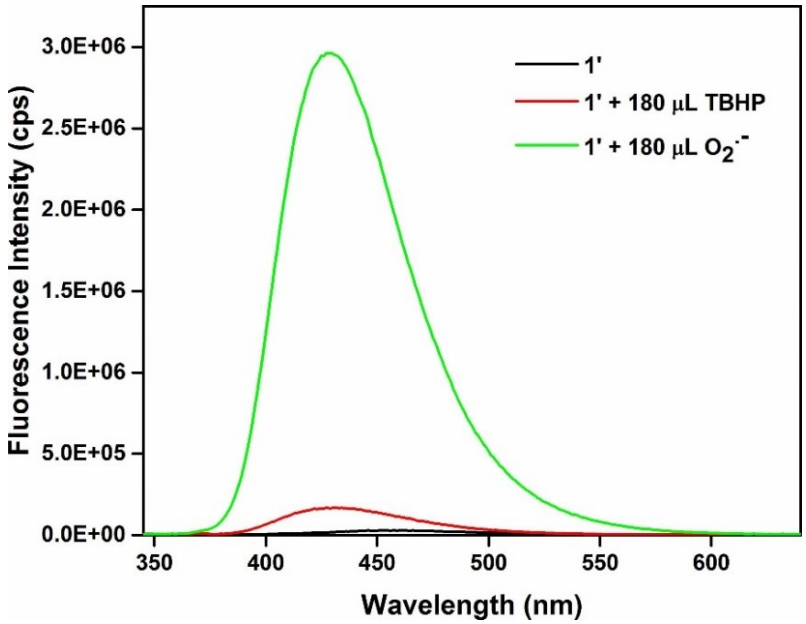

Figure S13. Change in the fluorescence intensity of **1′** upon addition of 10 mM TBHP solution (180 μL) in presence of $O_2^{\bullet-}$ mM (180 μL) solution.

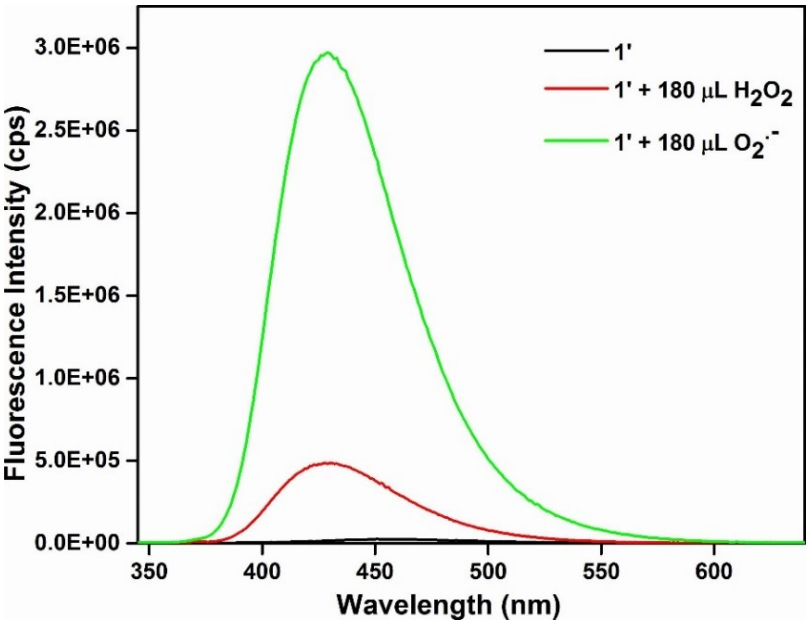

Figure S14. Change in the fluorescence intensity of **1′** upon addition of 10 mM H_2O_2 solution (180 μL) in presence of $O_2^{\bullet-}$ mM (180 μL) solution.

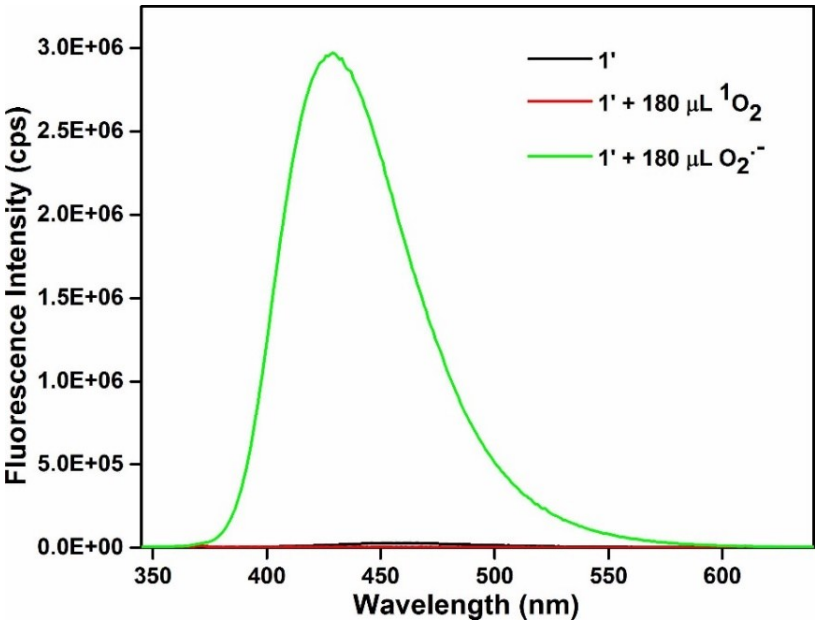

Figure S15. Change in the fluorescence intensity of **1′** upon addition of 10 mM $^1O_2$ solution (180 μL) in presence of $O_2^{\bullet-}$ (180 μL) solution.

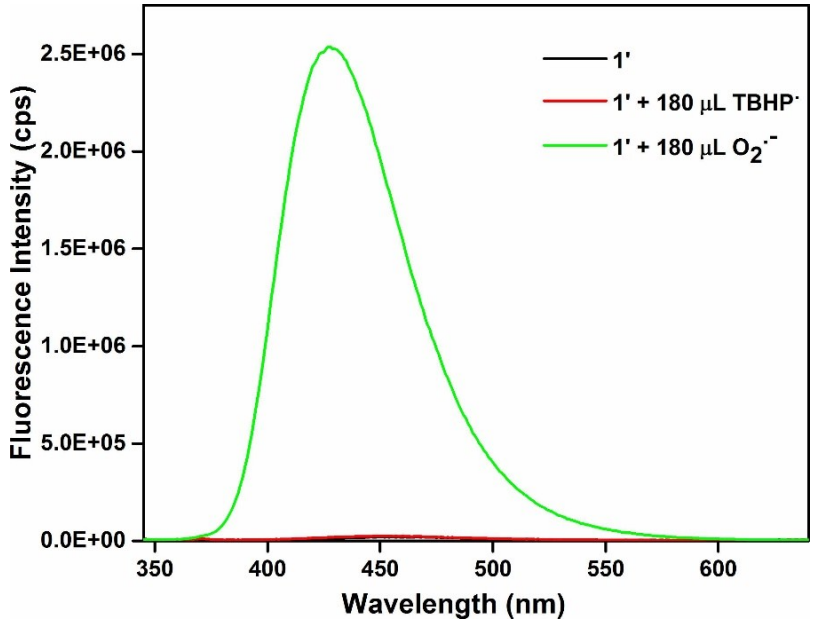

Figure S16. Change in the fluorescence intensity of **1′** upon addition of 10 mM TBHP$^{\bullet}$ solution (180 μL) in presence of $O_2^{\bullet-}$ mM (180 μL) solution.

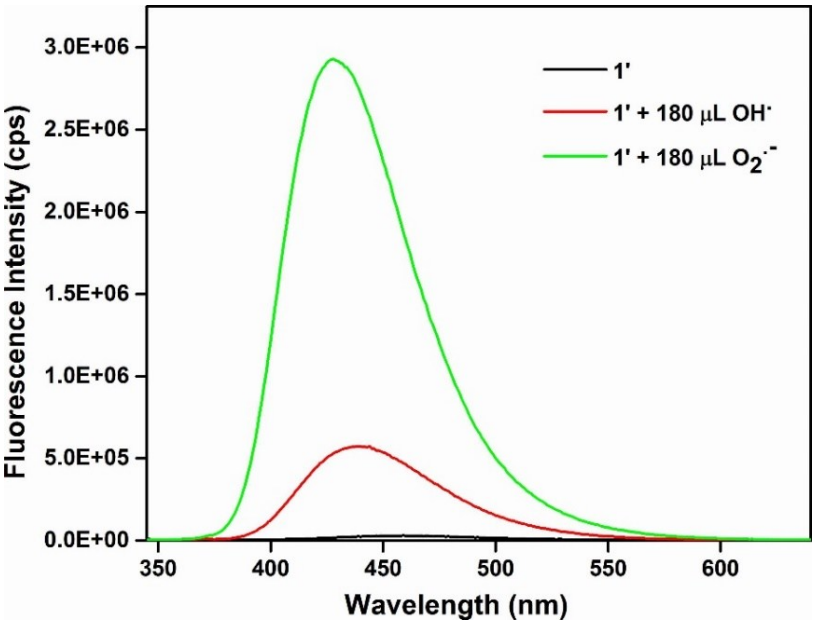

Figure S17. Change in the fluorescence intensity of **1′** upon addition of 10 mM $OH^{\bullet}$ radical solution (180 μL) in presence of $O_2^{\bullet-}$ mM (180 μL) solution.

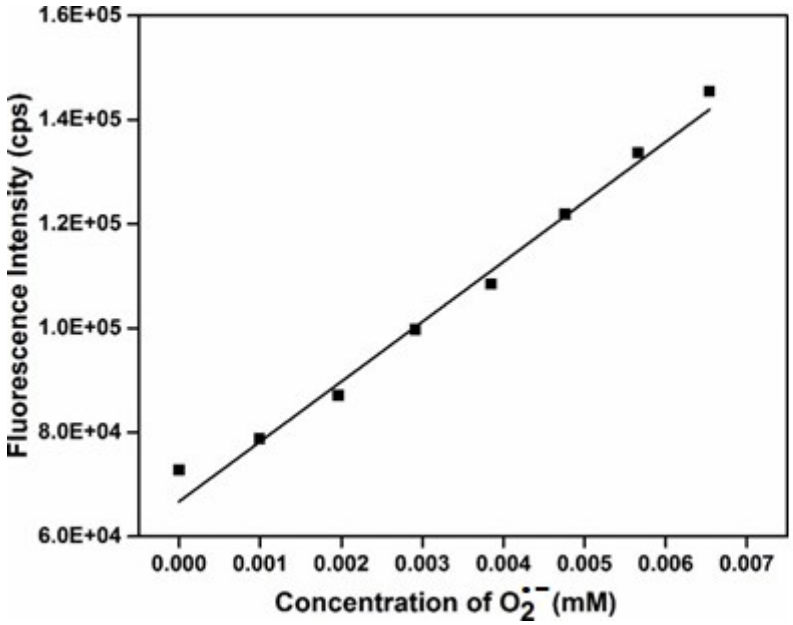

Figure 18. Change in the fluorescence intensity of **1′** in aqueous solution as a function of $O_2^{\bullet-}$ concentration.

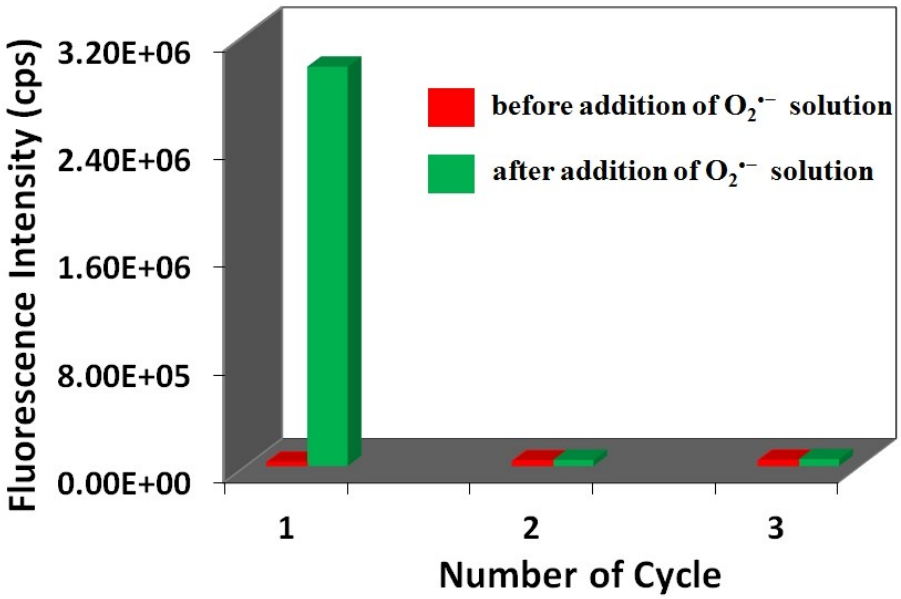

Figure S19. Recyclability plot of **1′** towards the sensing of $O_2^{\bullet-}$ in aqueous medium.

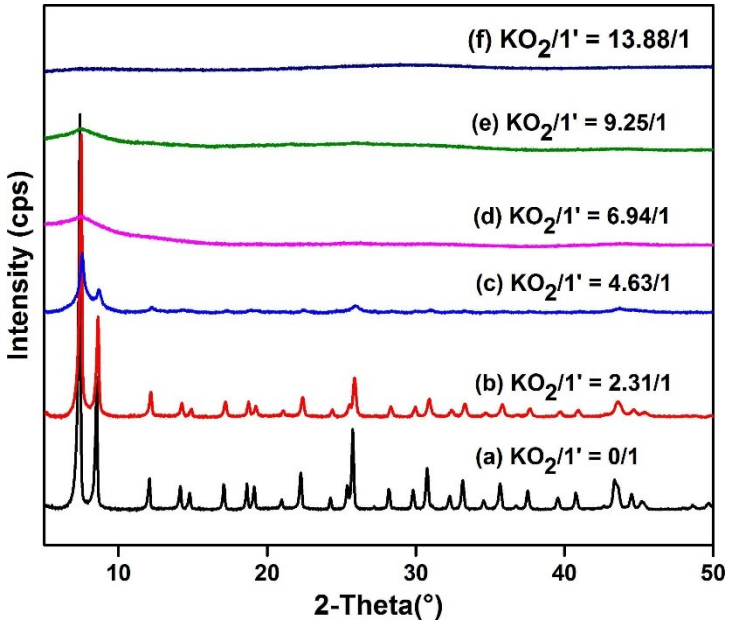

Figure S20. XRRD patterns of compound **1′** after treatment with different molar ratios of KO_2 with respect **1′**: **1′** after treatment with (a) KO_2/**1′** = 0.00, (b) KO_2/**1′** = 2.31, (c) KO_2/**1′** = 4.63, (d) KO_2/**1′** = 6.94, (e) KO_2/**1′** = 9.25, (f) KO_2/**1′** = 13.88.

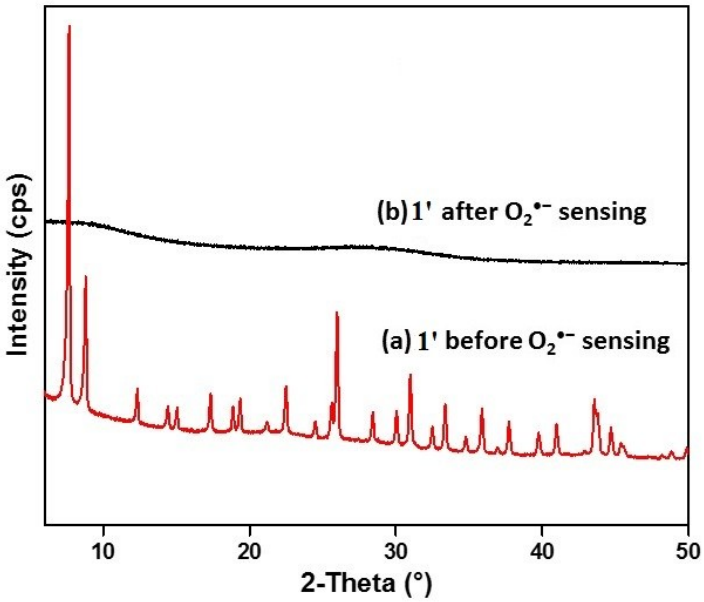

Figure S21. XRRD patterns of **1′** (a) before and (b) after $O_2^{\bullet-}$ sensing.

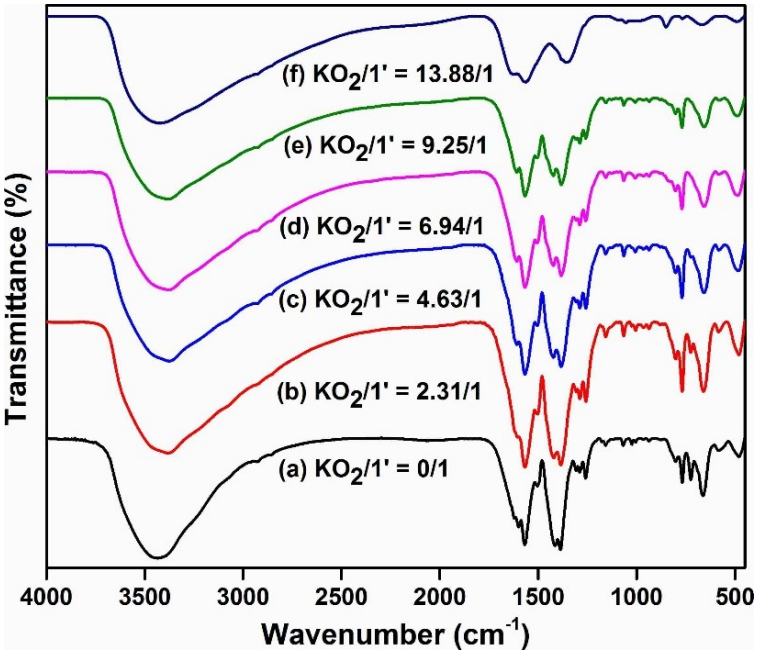

Figure S22. FT-IR spectra of compound **1′** after treatment with different molar ratios of KO_2 with respect **1′**: **1′** after treatment with (a) KO_2/**1′** = 0.00, (b) KO_2/**1′** = 2.31, (c) KO_2/**1′** = 4.63, (d) KO_2/**1′** = 6.94, (e) KO_2/**1′** = 9.25, (f) KO_2/**1′** = 13.88.

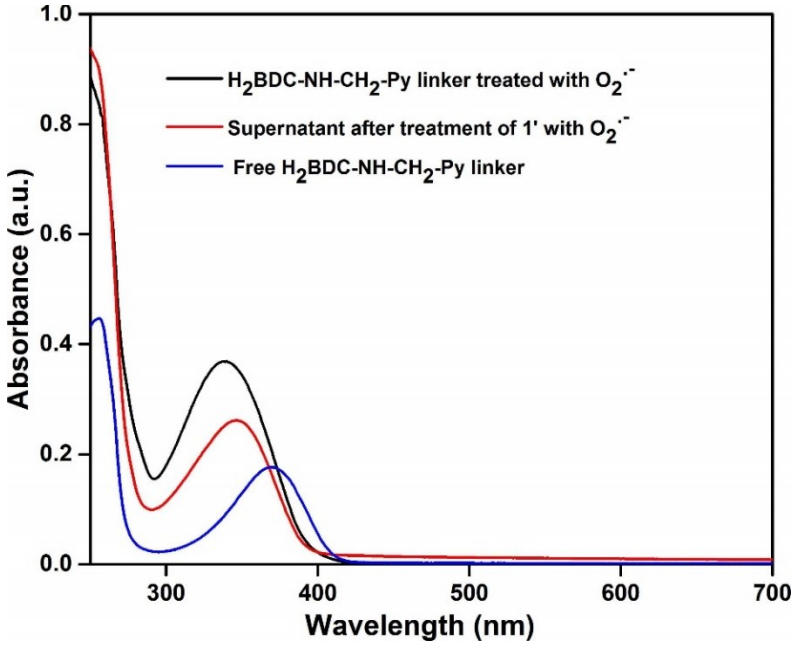

Figure S23. UV-Vis spectra of free $H_2BDC\text{-}NH\text{-}CH_2\text{-}Py$ (blue), supernatant after treatment of **1′** with $O_2^{\bullet-}$ (red) and free $H_2BDC\text{-}NH\text{-}CH_2\text{-}Py$ linker after treatment with $O_2^{\bullet-}$ (black) in methanol.

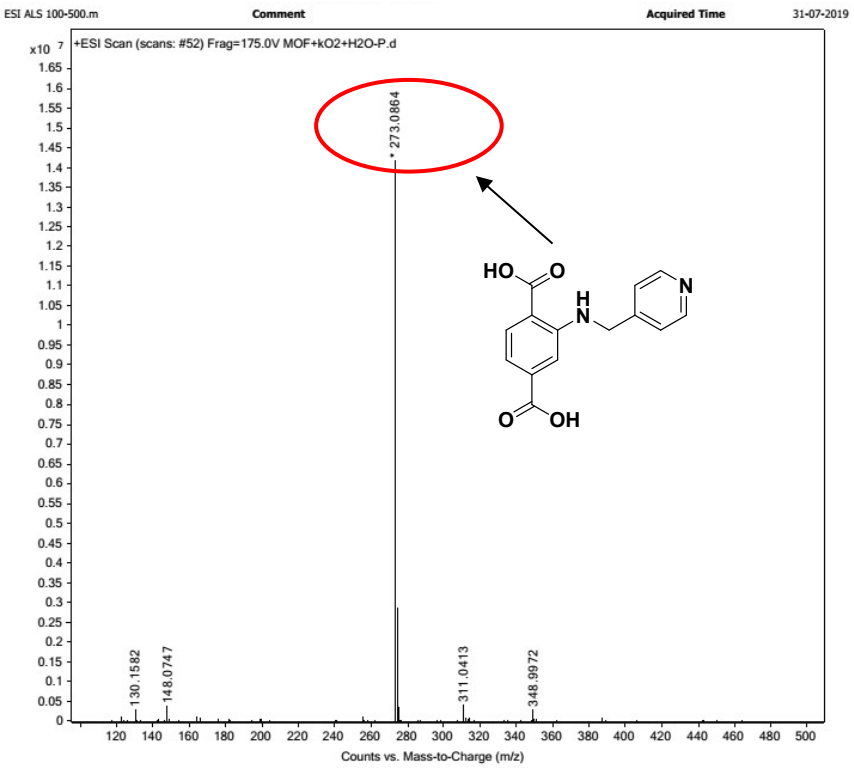

Figure S24. HR-MS spectrum of $O_2^{\bullet-}$-treated **1′** after digestion in MeOH/CsF. The spectrum shows m/z (positive ion mode) peak at 271.0706 which correspond to $(M+H)^+$ ion of $H_2BDC\text{-}C_6H_6N_2$ linker.

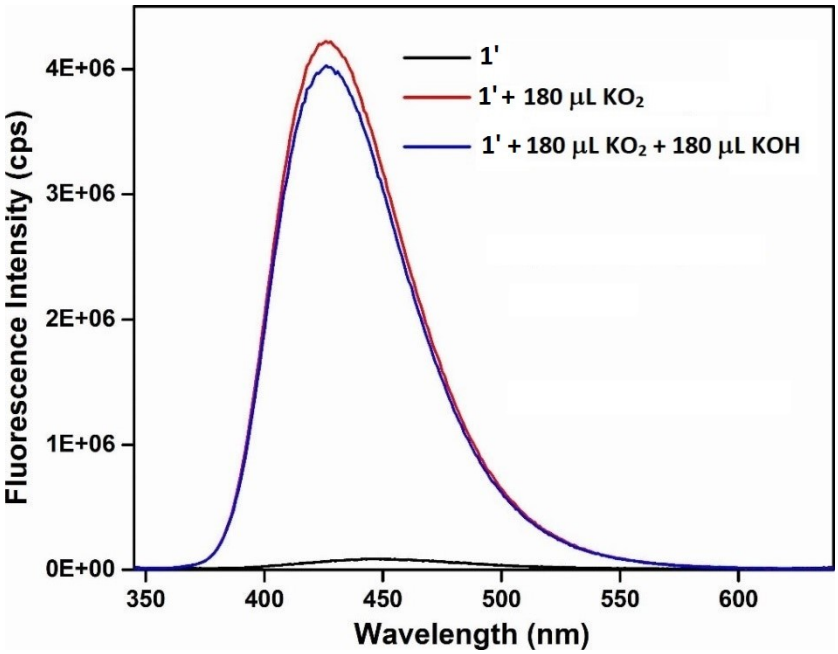

Figure S25. Change in the fluorescence intensity of **1′** upon addition of 10 mM KOH solution (180 µL) in presence of 10 mM $O_2^{\bullet-}$ solution (180 µL).

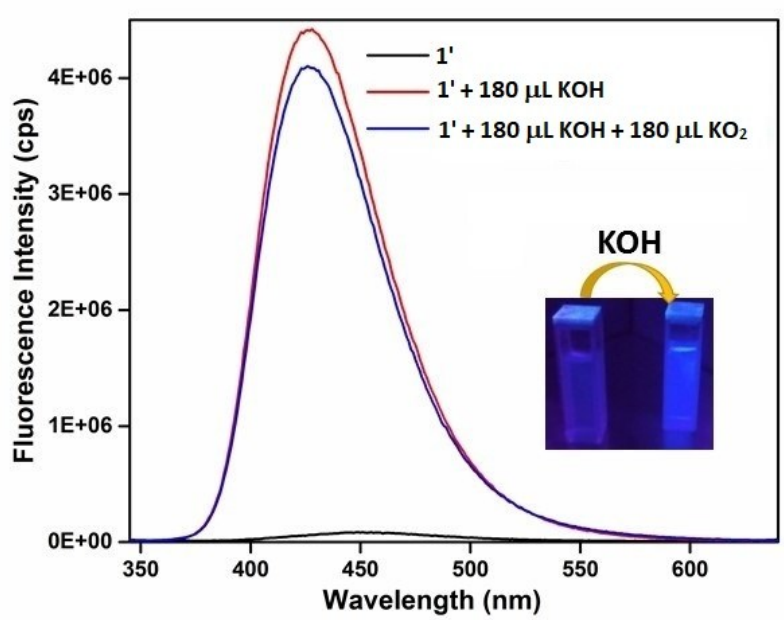

Figure S26. Change in the fluorescence intensity of **1′** upon addition of 10 mM $O_2^{\bullet-}$ solution (180 µL) in presence of 10 mM KOH solution (180 µL).

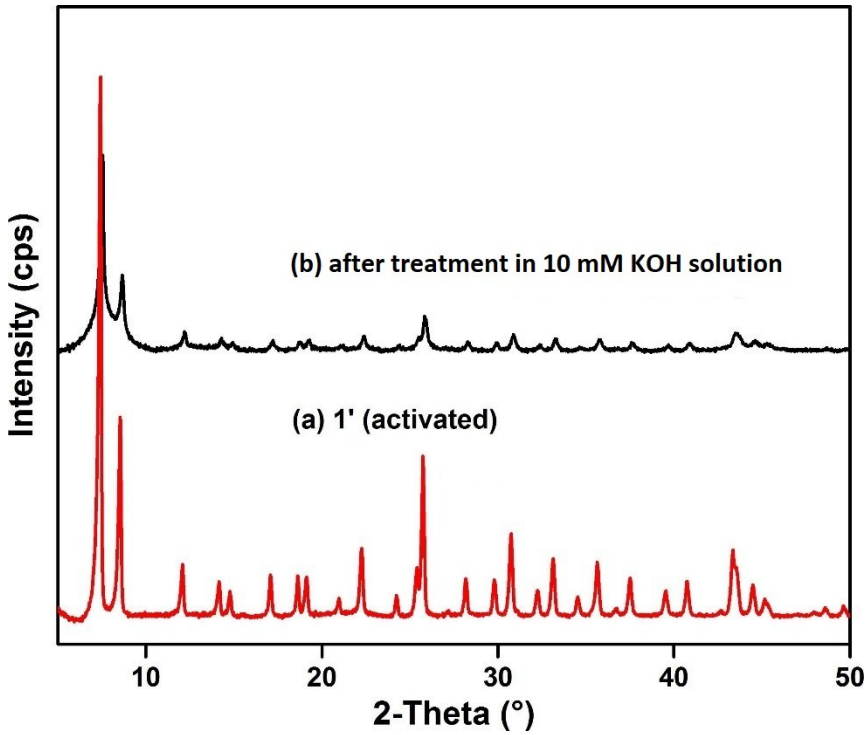

Figure S27. XRRD patterns of **1′** (a) before and (b) after treatment with 10 mM KOH solution (180 μL).

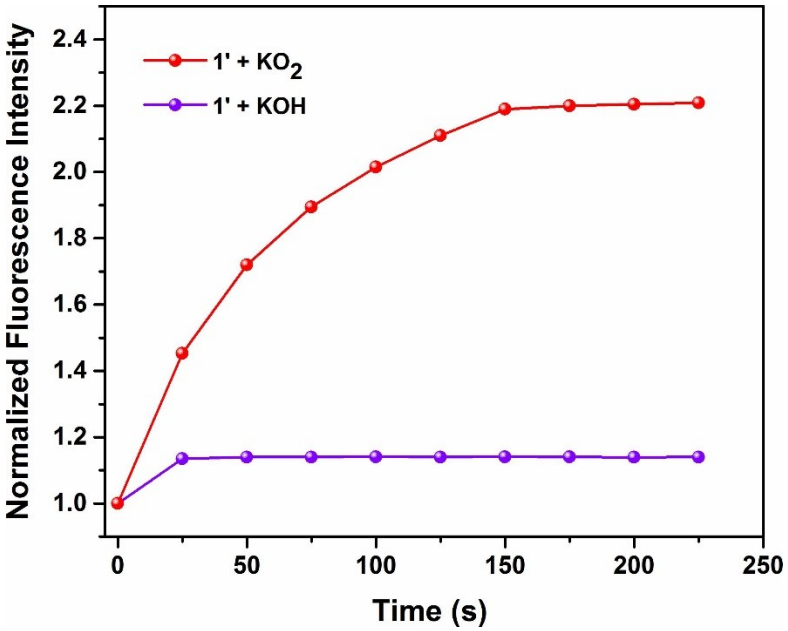

Figure S28. Fluorescence kinetics plots of **1′** upon treatment with 10 mM aqueous solutions of KO_2 (red) and KOH (violet).

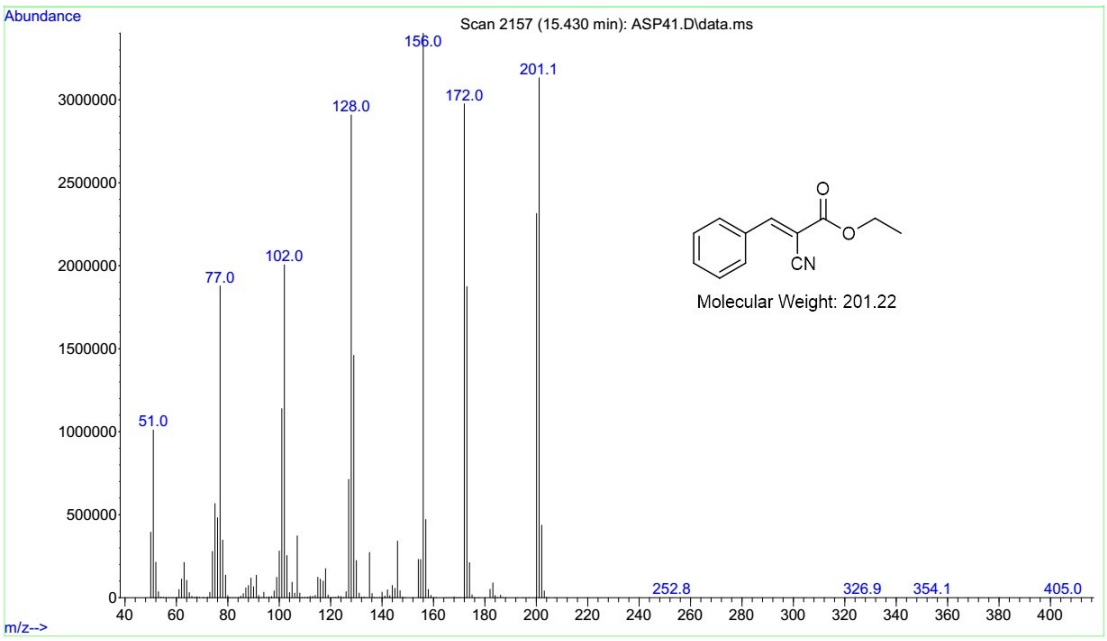

Figure S29. GC-MS trace of ethyl (*E*)-2-cyano-3-phenylacrylate.

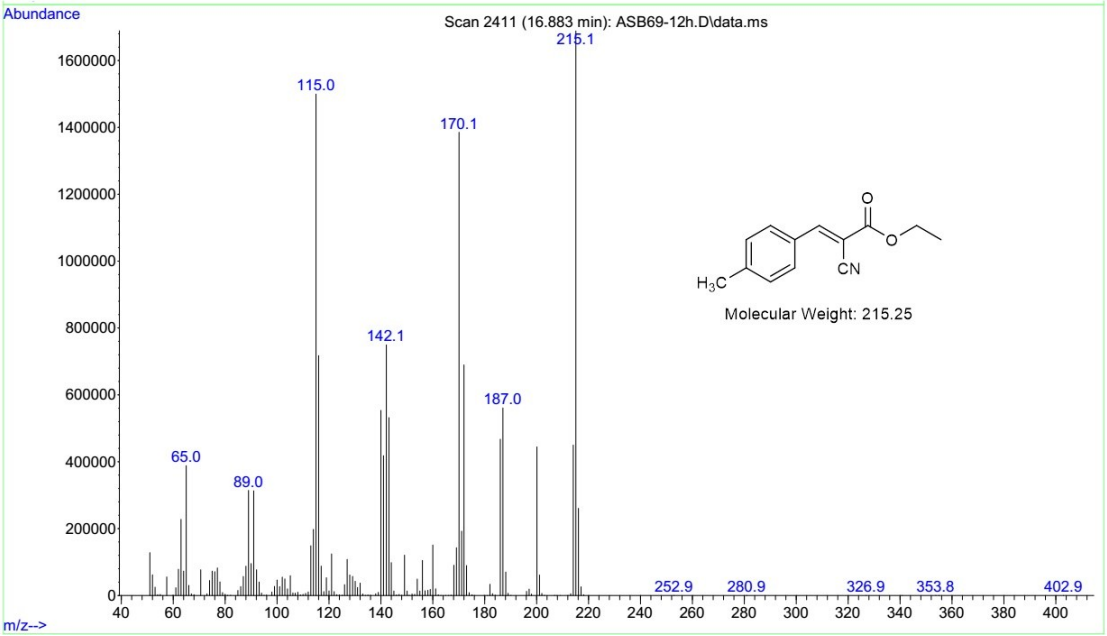

Figure S30. GC-MS trace of ethyl (*E*)-2-cyano-3-(*p*-tolyl)acrylate.

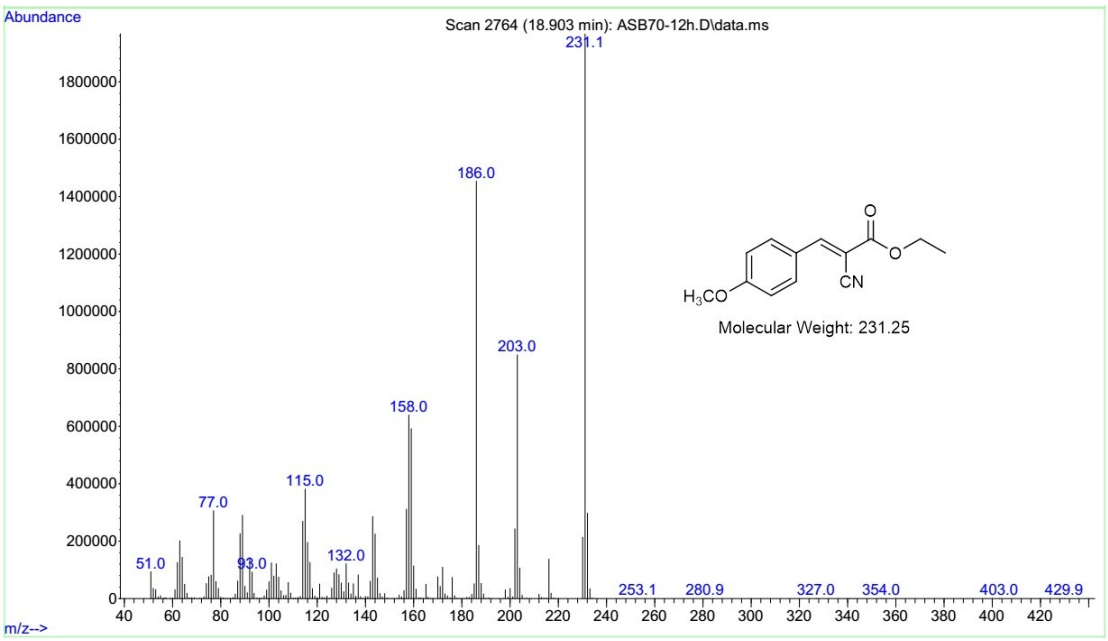

Figure S31. GC-MS trace of ethyl (*E*)-2-cyano-3-(4-methoxyphenyl)acrylate.

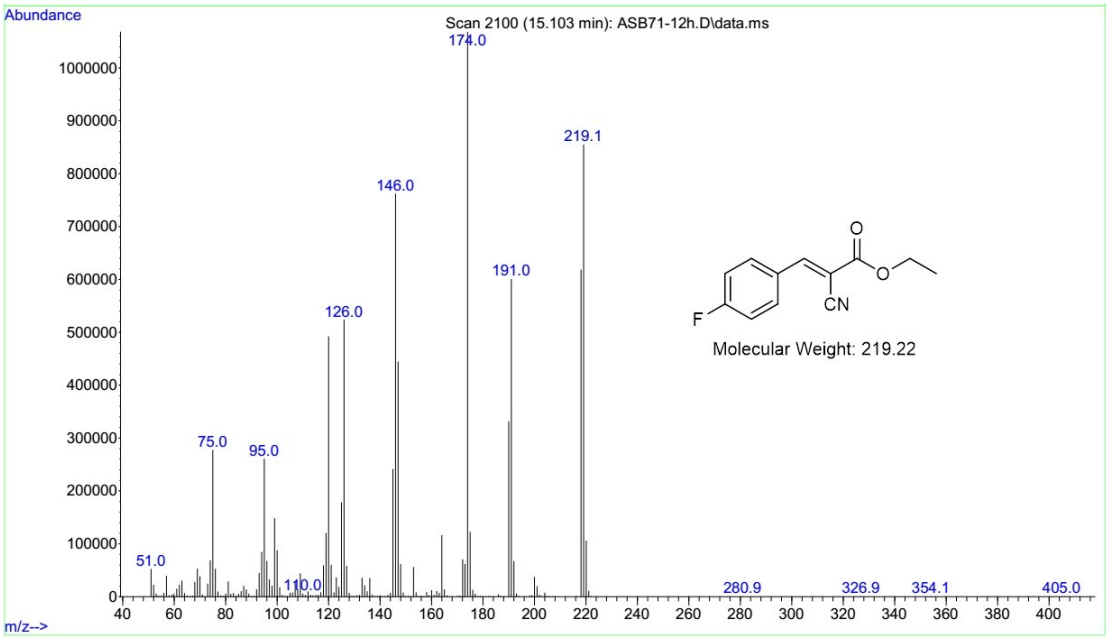

Figure S32. GC-MS trace of ethyl (*E*)-2-cyano-3-(4-fluorophenyl)acrylate.

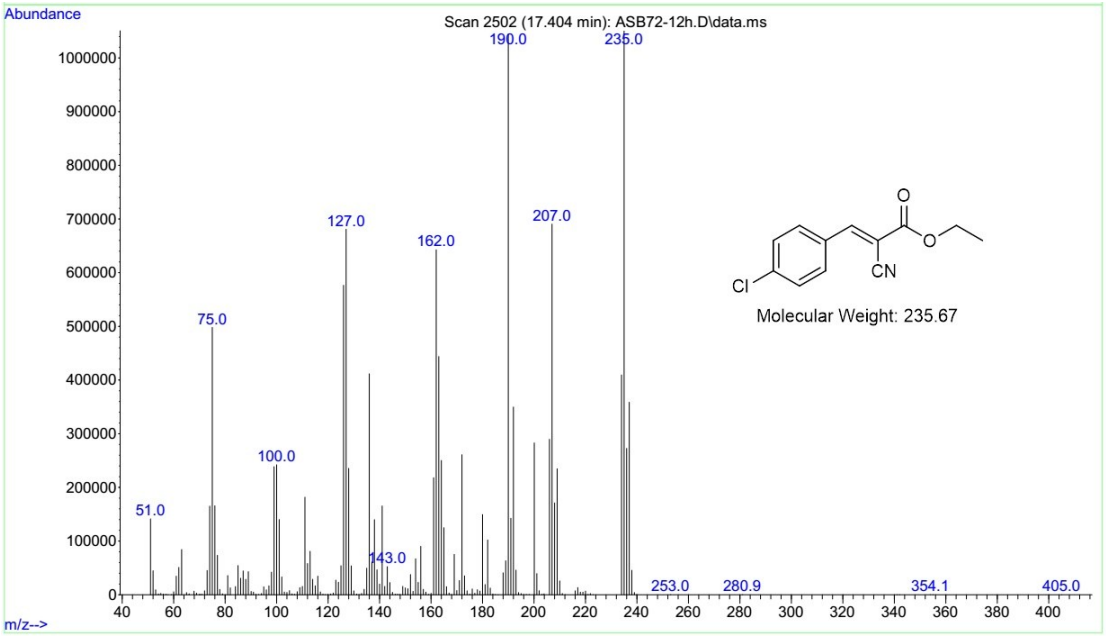

Figure S33. GC-MS trace of ethyl (*E*)-3-(4-chlorophenyl)-2-cyanoacrylate.

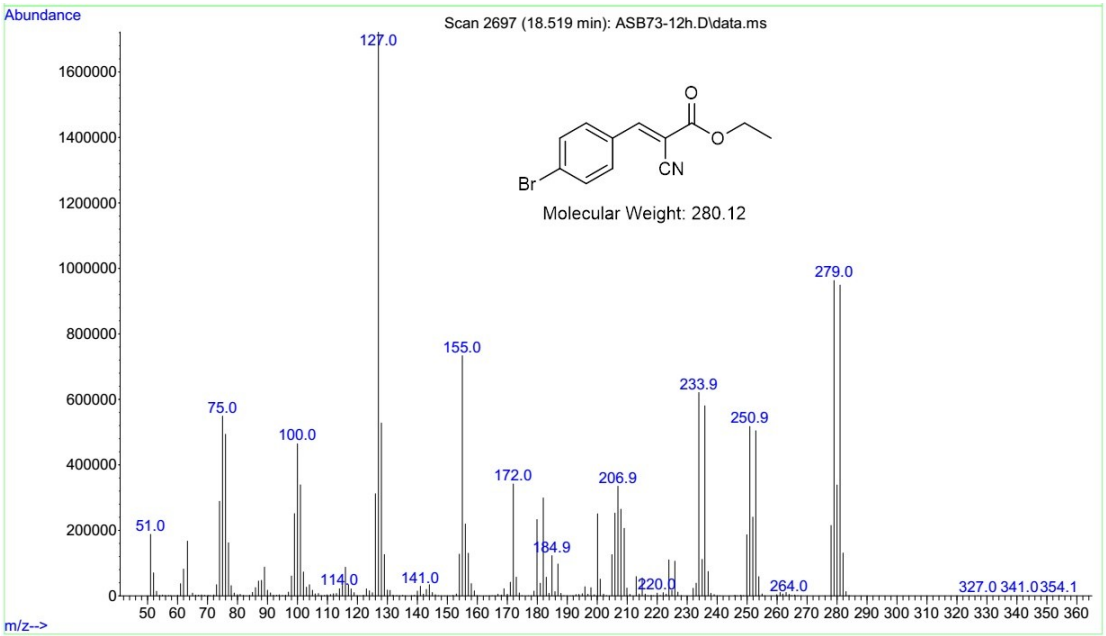

Figure S34. GC-MS trace of ethyl (*E*)-3-(4-bromophenyl)-2-cyanoacrylate.

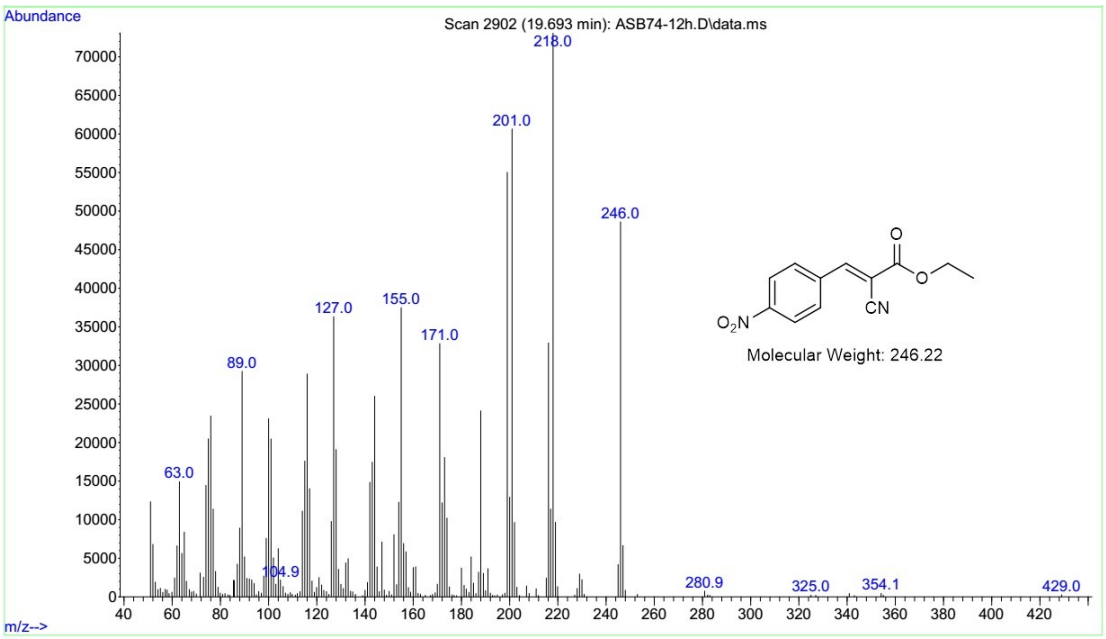

Figure S35. GC-MS trace of ethyl (*E*)-2-cyano-3-(4-nitrophenyl)acrylate.

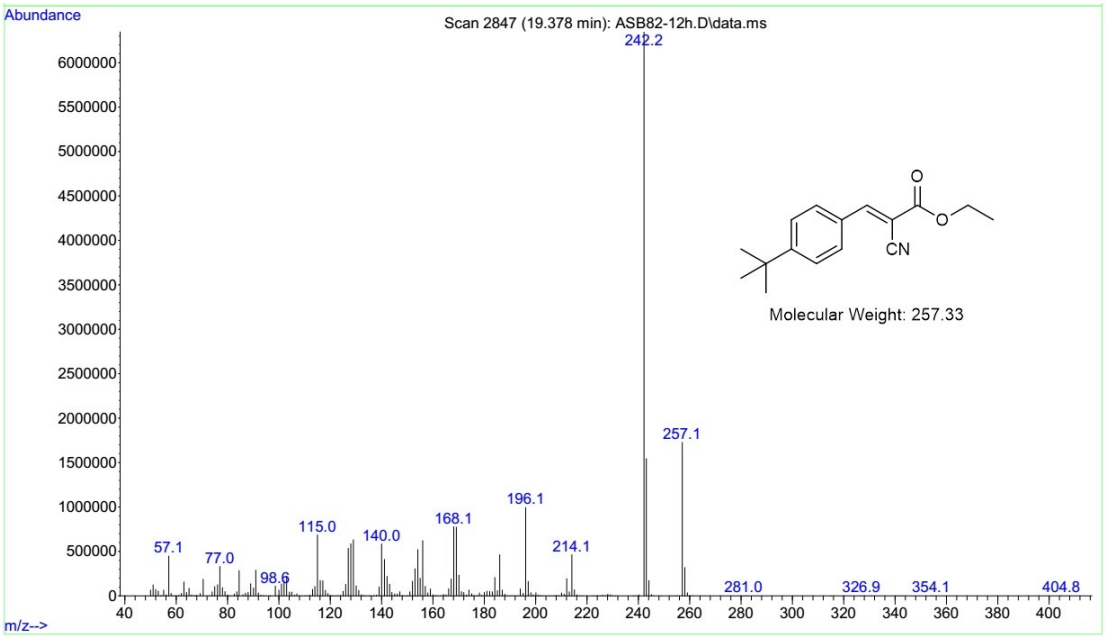

Figure S36. GC-MS trace of ethyl (*E*)-3-(4-(*tert*-butyl)phenyl)-2-cyanoacrylate.

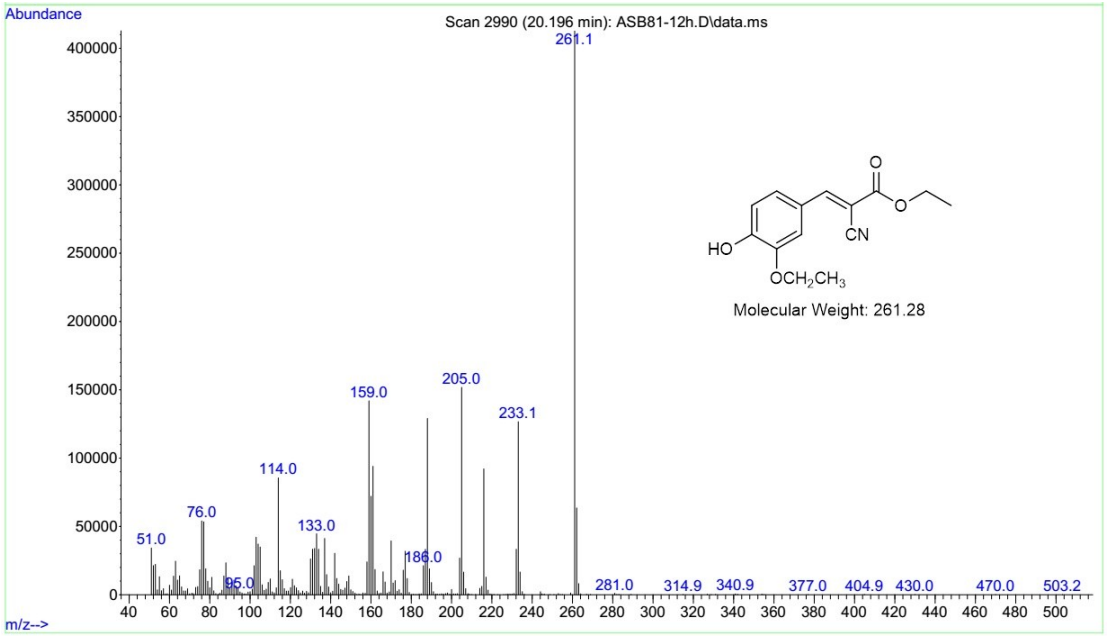

Figure S37. GC-MS trace of ethyl (*E*)-2-cyano-3-(3-ethoxy-4-hydroxyphenyl)acrylate.

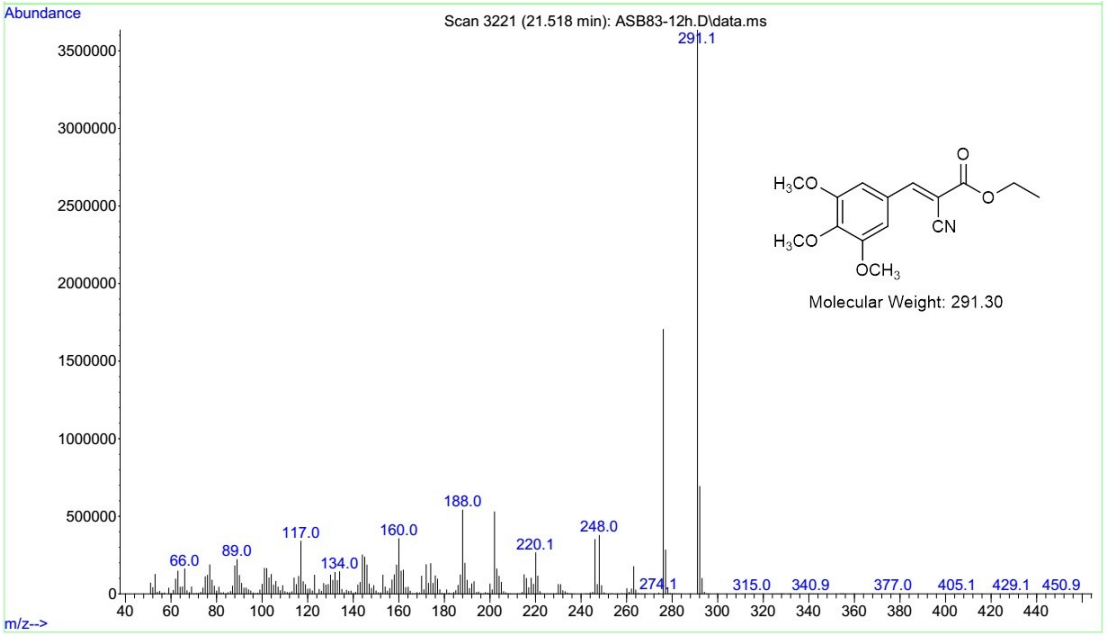

Figure S38. GC-MS trace of ethyl (*E*)-2-cyano-3-(3,4,5-trimethoxyphenyl)acrylate.

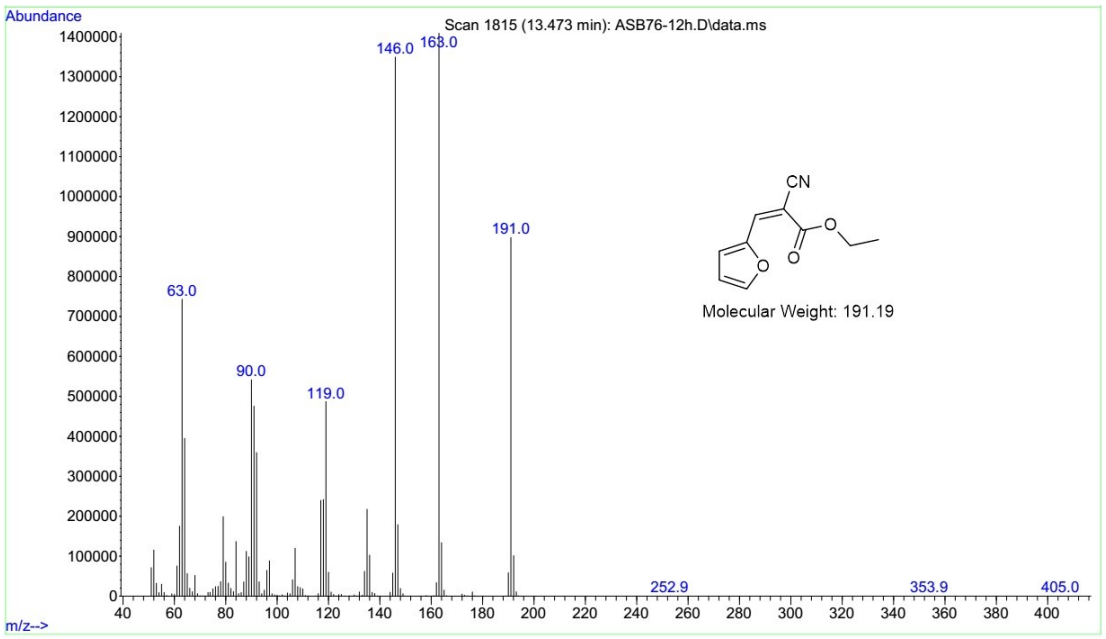

Figure S39. GC-MS trace of ethyl (*Z*)-2-cyano-3-(furan-2-yl)acrylate.

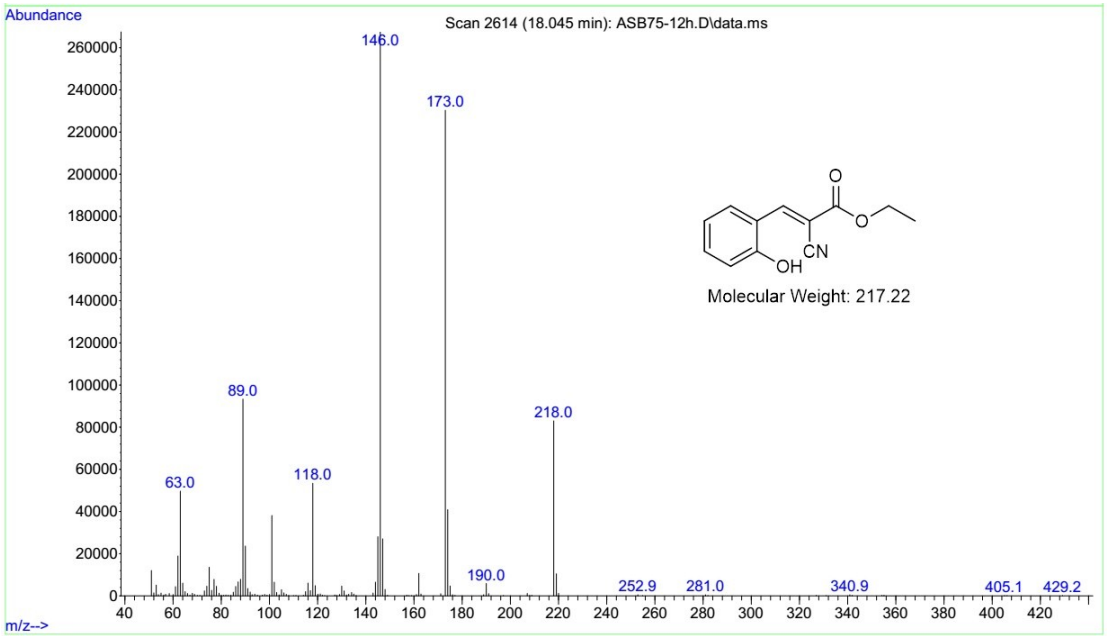

Figure S40. GC-MS trace of ethyl (*E*)-2-cyano-3-(2-hydroxyphenyl)acrylate.

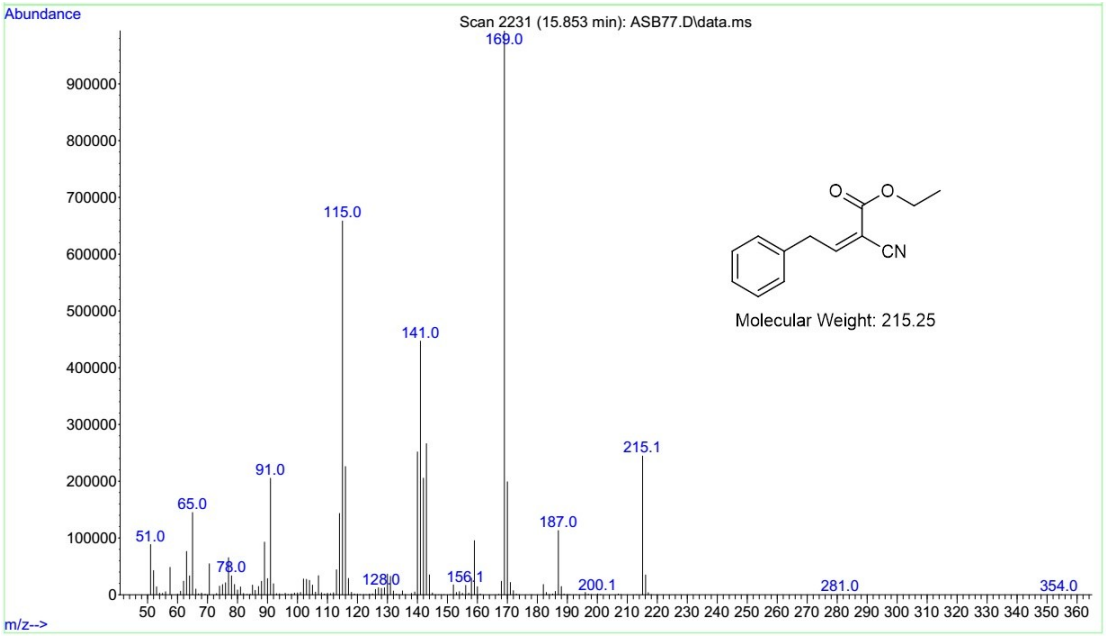

Figure S41. GC-MS trace of ethyl (*Z*)-2-cyano-4-phenylbut-2-enoate.

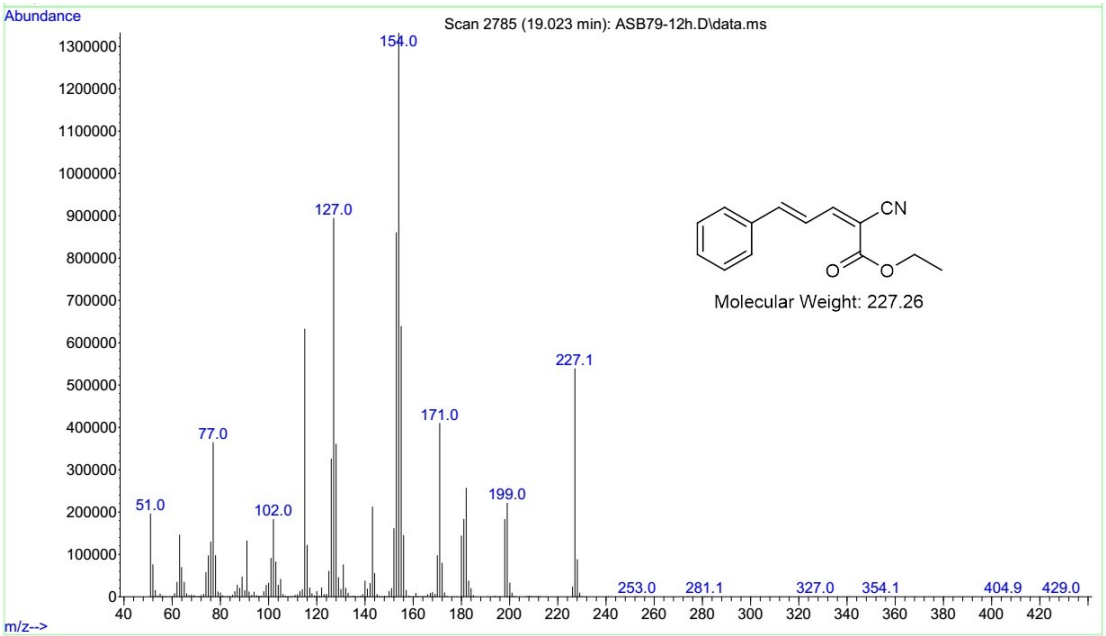

Figure S42. GC-MS trace of ethyl (2*Z*,4*E*)-2-cyano-5-phenylpenta-2,4-dienoate.

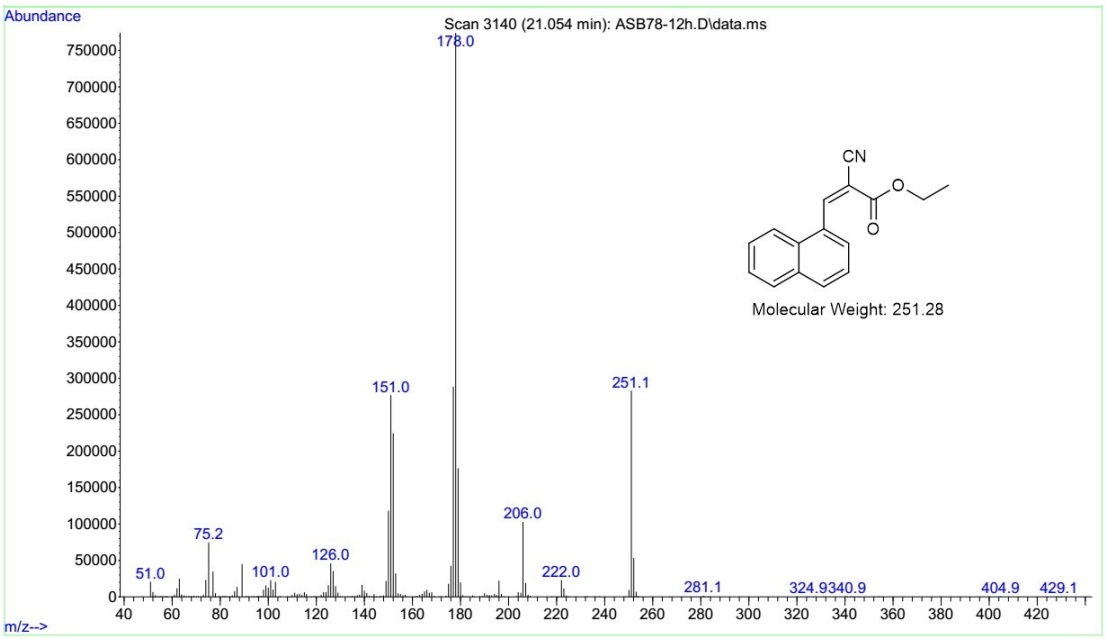

Figure S43. GC-MS trace of ethyl (*Z*)-2-cyano-3-(naphthalen-1-yl)acrylate.

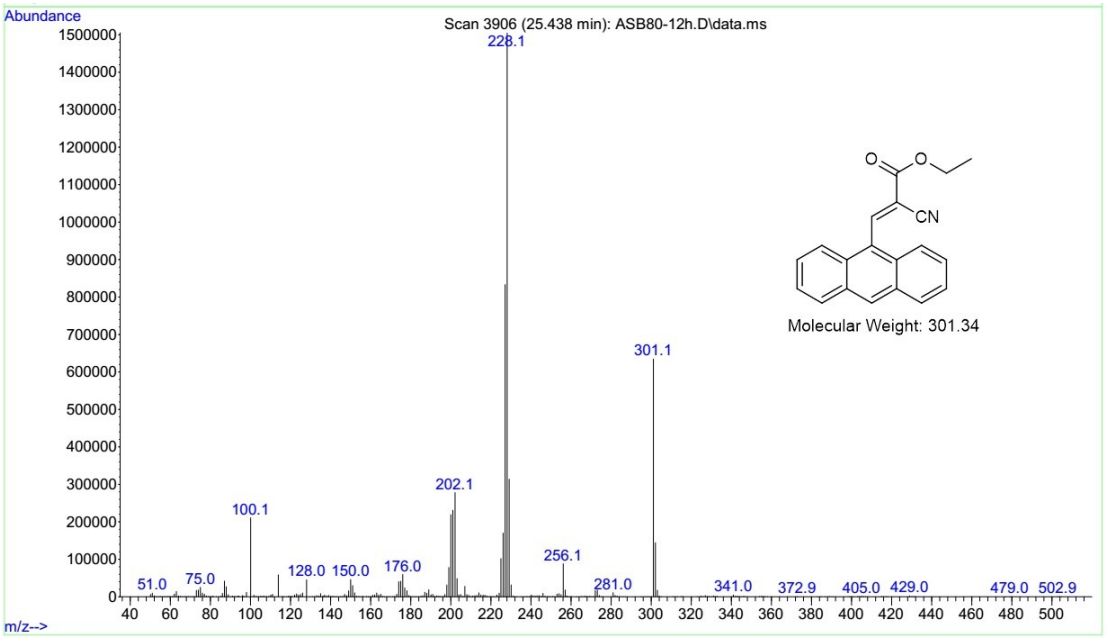

Figure S44. GC-MS trace of ethyl (*E*)-3-(anthracen-9-yl)-2-cyanoacrylate.

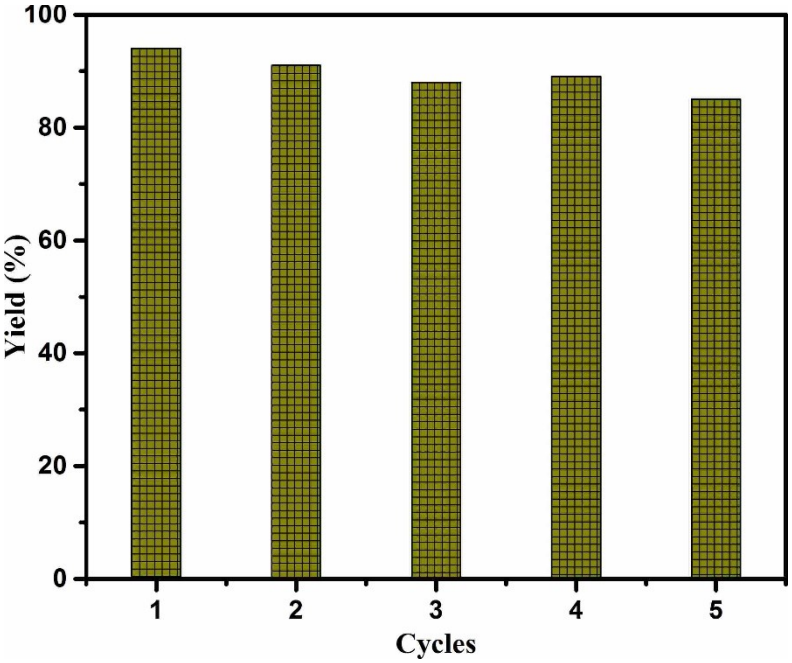

Figure S45. Reusability plot for the Knoevenagel condensation between benzaldehyde and ethyl cyanoacetate using **1′** as a heterogeneous solid base catalyst.

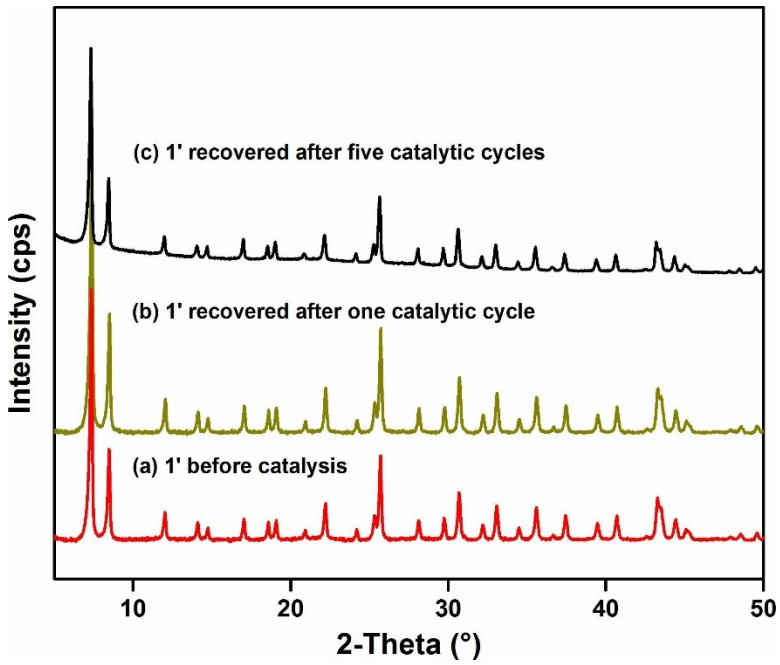

Figure S46. XRPD patterns of **1′** (a) before catalysis, (b) recovered after one catalytic cycle and (c) recovered after five catalytic cycles.

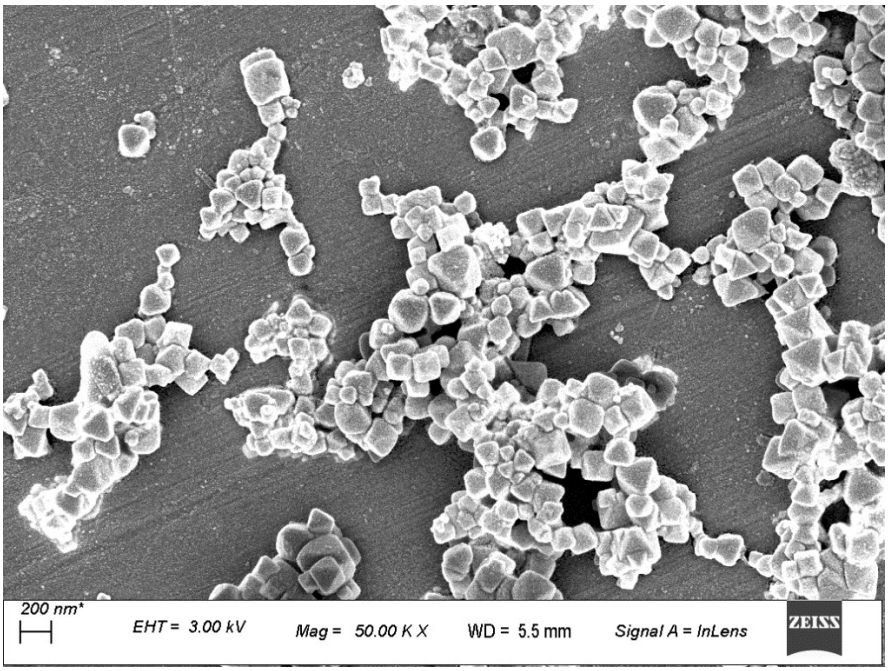

Figure S47. FE-SEM images of as-synthesized **1**.

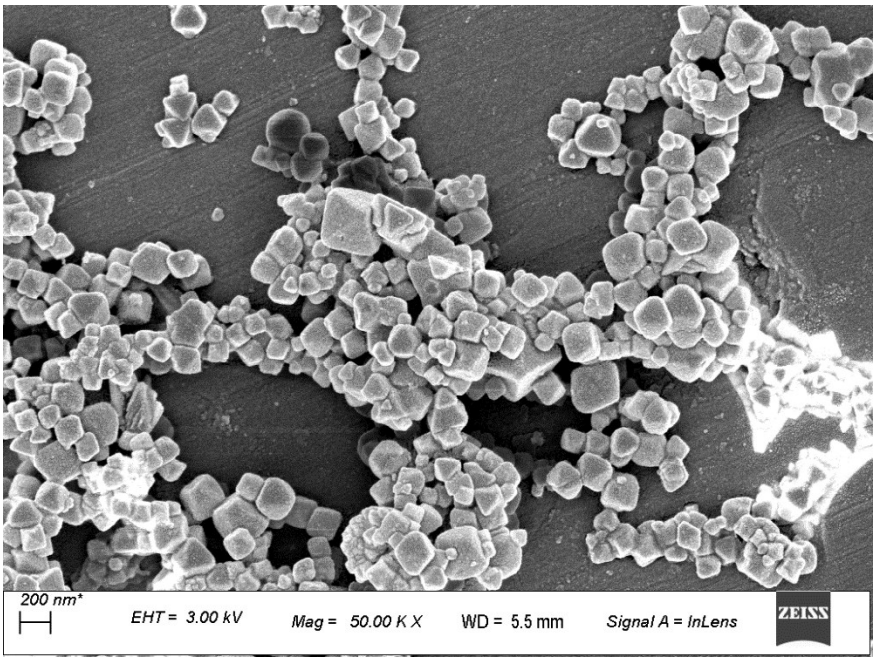

Figure S48. FE-SEM images of **1′** before catalysis.

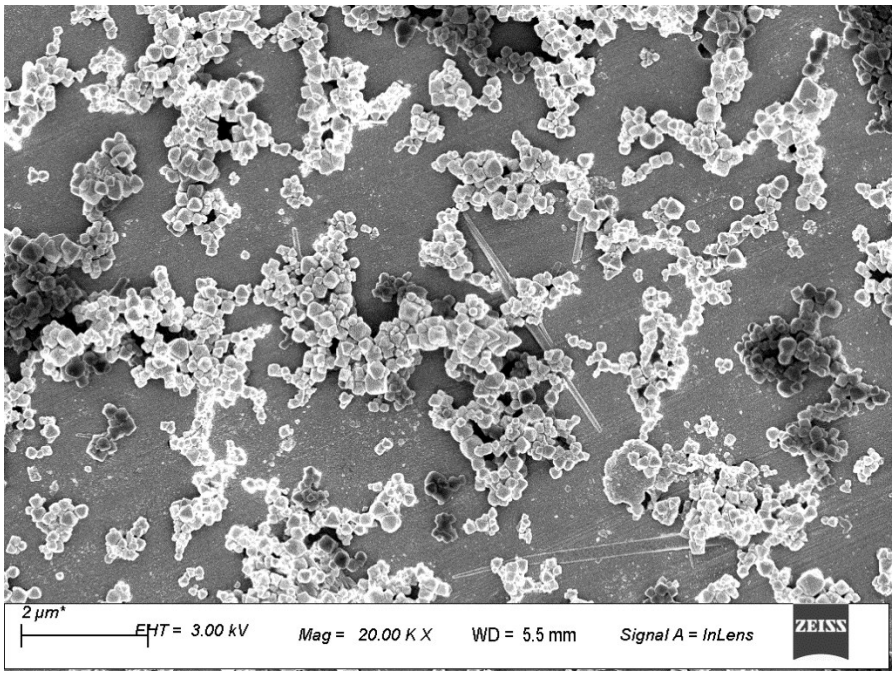

Figure S49. FE-SEM images of **1′** recovered after five catalytic cycles.

Table S1. Unit cell parameters of as-synthesized Zr-UiO-66-NH-CH_2-Py obtained by indexing its XRPD pattern. The obtained values were compared with those of the previously reported un-functionalized and functionalized Zr-UiO-66 MOF.

Compound Name	Zr-UiO-66-NH-CH_2-Py MOF (this work)	Zr-UiO-66 MOF (reported)[2]
Crystal System	cubic	cubic
a = b = c (Å)	20.755(3)	20.7004(2)
V (Å^3)	8940.3(21)	8870.3(2)

Table S2. Comparison of the detection limit, response time, nature of fluorescence change and solvent system used for $O_2^{\bullet-}$ detection for probes reported till date.

Sl. No.	Name of Probe	Detection Limit (nM)	Response Time (s)	Medium Used	Nature of Fluorescence Change	Ref.
1	6-(benzo[d]thiazol-2-yl)naphthalen-2-yl trifluoromethanesulfonate	1	300	PBS (10 mM, pH = 7.4) DMSO (2%, v/v) solution	turn-on	3
2	PS-SO_3H@Tb/G NCPs	3.4	–	Tris-HCl (50 mM, pH = 8)	turn-off	4
3	BDP	70.5	120	PBS/DMSO (v/v, 3.5/6.5, pH = 7.4)	turn-on	5
4	NS-O	1710	120	PBS/DMSO (v/v = 1/1, pH 7.4)	turn-on	6
5	PNF-1	9.9	600	HEPES	turn-on	7
6	DBZTC	1.68	600	HEPES (10 mM, pH = 7.40)	turn-on	8
7	Zr-UiO-66-NH-CH_2-Py MOF	210	240	water	turn-on	this work

References:

1. L. G.-Tovar, S. R.-Hermida, I. Imaz and D. Maspoch, *J. Am. Chem. Soc.*, 2017, **139**, 897-903.
2. J. H. Cavka, S. Jakobsen, U. Olsbye, N. Guillou, C. Lamberti, S. Bordiga and K. P. Lillerud, *J. Am. Chem. Soc.*, 2008, **130**, 13850–13851.
3. D. Lu, L. Zhou, R. Wang, X.-B. Zhang, L. He, J. Zhang, X. Hu and W. Tan, *Sens. Actuators, B*, 2017, **250**, 259–266.
4. Y. Song, J. Hao, D. Hu, M. Zeng, P. Li, H. Li, L. Chen, H. Tan and L. Wang, *Sens. Actuators, B*, 2017, **238**, 938–944.
5. J. Yang, X. Liu, H. Wang, H. Tan, X. Xie, X. Zhang, C. Liu, X. Qu and J. Hua, *Analyst*, 2018, **143**, 1242–1249.
6. Y. Xuan and J. Qu, *RSC Adv.*, 2018, **8**, 4125–4129.
7. K. Xu, X. Liu and B. Tang, *ChemBioChem*, 2007, **8**, 453–458.
8. J. J. Gao, K. H. Xu, B. Tang, L. L. Yin, G. W. Yang and L. G. An, *FEBS J.*, 2007, **274**, 1725–1733.